Journal of Sound and Vibration 329 (2010) 5070–5086

Contents lists available at ScienceDirect

Journal of Sound and Vibration

journal homepage: www.elsevier.com/locate/jsvi

Structural damage detection using cross correlation functions of vibration response

Le Wang [a,*], Zhichun Yang [a], T.P. Waters [b]

[a] School of Aeronautics, Northwestern Polytechnical University, Xi'an 710072, China
[b] Institute of Sound and Vibration Research, University of Southampton, Highfield, Southampton SO17 1BJ, UK

ARTICLE INFO

Article history:
Received 14 September 2009
Received in revised form
22 April 2010
Accepted 22 June 2010
Handling Editor: I. Trendafilova

ABSTRACT

Structural damage detection methods based on vibration responses are appealing for a variety of reasons such as their potential to observe damage from sensors placed remote from an unknown damage site. Of particular interest to the authors is online damage detection in which changes in the structure can be flagged up in an automated fashion by permanently installed transducers. In a previous paper by the authors, the inner product vector (IPV) was proposed as a damage detection algorithm which uses cross correlation functions between response measurements. Implicitly assumed in the formulation is that the response quantity is that of displacement resulting from white noise excitation. In this paper, the IPV technique is first reviewed and then generalised to address velocity and acceleration response to band pass white noise excitation. It is shown that the IPV is a weighted summation of the mode shapes, and the effect of some particular measurement noise on the IPV can be adaptively eliminated in the calculation of IPV. Then, the damage detection method based on changes in the IPV is proposed. Finally, damage detection experiments of shear frame structure, honeycomb sandwich composite beam and aircraft stiffened panel are presented to illustrate the feasibility and effectiveness of the proposed method.

1. Introduction

Investigations of structural damage detection based on vibration testing have been hot topics in recent decades [1–4]. Depending upon whether a precise analytical model of the structure is required, vibration based structural damage detection methods can be classified as model based structural damage detection methods or non-model based structural damage detection methods. In model based structural damage detection methods, such as the investigations of Li and Law [5], Park [6], Dilena and Morassi [7], Dyke and Koh [8] and Yu et al. [9], a model updating procedure is always needed. This might be a complex task requiring either model reduction or modal expansion [10] and regularization of a potentially ill-conditioned updating matrix [11]. Non-model based structural damage detection methods are used to avoid some of the drawbacks of model based structural damage detection methods. In non-model based structural damage detection methods, a precise analytical model of the structure is not required, and the damage feature is directly extracted from the dynamic responses or modal parameters. As the computation task is usually not so complex in non-model based structural damage detection methods, it can be easily performed in online damage detection. Generally speaking, there are also two types of non-model based structural damage detection methods. The first method is based on modal parameters extracted

* Corresponding author. Tel./fax: +86 29 8846 0461.
E-mail addresses: wanglnpu@126.com, wangle@mail.nwpu.edu.cn (L. Wang).

0022-460X/$ - see front matter Crown Copyright © 2010 Published by Elsevier Ltd. All rights reserved.
doi:10.1016/j.jsv.2010.06.020

Nomenclature

C_k bandwidth of the band pass white noise excitation at point k
$C_{k,c}$ central frequency of C_k
$\mathbf{D}_{\mathrm{IPV}}$ change in normalized IPVs between the intact and damaged structures
$\mathbf{D}'_{\mathrm{IPV}}$ the first-order difference of $\mathbf{D}_{\mathrm{IPV}}$
$\mathbf{D}''_{\mathrm{IPV}}$ the second-order difference of $\mathbf{D}_{\mathrm{IPV}}$
f_k excitation force at point k
$G_{j,r}$ coefficient dependent on the rth modal parameters and response measurement point j
g_r impulse response function related to parameters of rth mode
m_r rth modal mass
n number of modes
p number of the measurement point
$R_{x_i x_j}$ cross correlation function of response x_i and x_j under all excitations
$R_{x_i x_j f_k}$ cross correlation function of response x_i and x_j under the excitation f_k
$\mathbf{R}^{\mathrm{dis}}_{\mathrm{IPV}}$ IPV calculated from displacements
$\mathbf{R}^{\mathrm{vel}}_{\mathrm{IPV}}$ IPV calculated from velocities
$\mathbf{R}^{\mathrm{acc}}_{\mathrm{IPV}}$ IPV calculated from accelerations
$\overline{\mathbf{R}}$ normalized IPV
$R^{u}_{\mathrm{IPV},i}$ ith element of normalized IPV of the intact structure
$R^{d}_{\mathrm{IPV},i}$ ith element of normalized IPV of the damaged structure
t time
T time lag
x_{ik} displacement at point i due to excitation at point k
α_c coefficient corresponding to a confidence interval
α_k one-side auto-spectral density of white noise excitation at point k
$\beta^{\mathrm{dis}}_{k,rs}$, $\beta^{\mathrm{vel}}_{k,rs}$, $\beta^{\mathrm{acc}}_{k,rs}$ coefficients dependent on the rth and sth modal parameters, the one-side auto-spectral density α_k, bandwidth C_k and central frequency $C_{k,c}$ of the band bass white noise
δ Dirac Delta function
ζ_r rth modal damping
$\zeta^{\mathrm{dis}}_{j,r}$, $\zeta^{\mathrm{vel}}_{j,r}$, $\zeta^{\mathrm{acc}}_{j,r}$ weighting factors dependent on the reference response measurement point j, the rth modal parameters and all the band pass white noise excitations
ϑ_r phase dependent on the rth modal parameters
$\kappa^{\mathrm{dis}}_{j,r}$, $\kappa^{\mathrm{vel}}_{j,r}$, $\kappa^{\mathrm{acc}}_{j,r}$ coefficients dependent on the rth modal parameters and the response measurement point j and the excitation positions
λ_1, λ_2 integral variable
μ_D mean value of damage index
σ integral variable
σ_D standard deviation of damage index
τ integral variable
ϕ_{ir} ith element in the rth mode shape
ω_{dr} rth damped modal frequency
ω_{nr} rth modal frequency
$\mathrm{E}[\cdot]$ expectation operator
$\mathrm{RMS}(\cdot)$ root mean square value operator

Subscript

i response measurement point
j reference response measurement point
k excitation point
r rth mode
s sth mode

Superscript

dis parameter related to IPV calculated from displacements
vel parameter related to IPV calculated from velocities
acc parameter related to IPV calculated from accelerations

from time domain or frequency domain responses (such as investigations of Kim et al. [12], Dilena and Morassi [13], Alvandi and Cremona [14], Choi et al. [15], Wong et al. [16]), and the damage is detected from the differences between the measured modal parameters of the current and intact structures. The other method is based on time domain responses or frequency domain responses directly (such as investigations of Worden et al. [17], Manson et al. [18], Pierce et al. [19], Wang and Ren [20], Fassois and Sakellarou [21],Trendafilova and Manoach [22]), and the damage is detected from the differences between the measured time domain or frequency domain responses of the current and intact structures.

In the field of non-model based structural damage detection methods, the authors of this paper have previously proposed a damage detection method based on the inner product vector (IPV) of displacements. The IPV is related to the mode shapes and can be directly calculated from the time domain vibration responses to white noise excitation. The effectiveness and veracity of the proposed method were demonstrated by numerical simulation results of delamination damage detection for a composite laminate beam [23]. As the IPV can be directly calculated by time domain vibration response, and the damages are located by the local maximum of the damage index defined by the IPV, the IPV-based structural damage detection method can be potentially used as an online damage detection method. In our foregoing research, the theory of IPV is based on the cross correlation functions of displacement response under white noise excitation. However, in practice we can only obtain band pass white noise excitation and it may also be easier to measure other types of response (such as velocity or acceleration). The research in this paper addresses these limitations.

In this paper, firstly, the definition of the IPV is reviewed. Then the influences of response type, excitation frequency bandwidth, and measurement noise on the IPV are studied. Thirdly, the IPV-based structural damage detection method is

proposed. And then, experimental examples of stiffness reduction detection of shear frame structure, debonding damage detection of honeycomb sandwich composite beam and bolt loosening detection of aircraft stiffened panel are adopted to illustrate the feasibility and effectiveness the IPV-based structural damage detection method. Finally, some conclusions are summarized.

2. Theory of inner product vector

2.1. Inner product vector

The inner product vector is based on the modal identification technique known as Natural Excitation Technique (NExT), in which it is exploited that the cross correlation functions between two responses under white noise excitation have the form of the impulse response function [24,25]. Thus, the NExT is reviewed prior to the review of the inner product vector for displacement responses. Then, inner product vector is reviewed and generalised to address velocity and acceleration response.

2.1.1. Natural excitation technique (NExT)

Assuming zero initial conditions, the displacement $x_{ik}(t)$ at point i due to excitation $f_k(t)$ at point k is

$$x_{ik}(t)=\sum_{r=1}^{n}\phi_{ir}\phi_{kr}\int_{-\infty}^{t}f_k(\tau)g_r(t-\tau)\,\mathrm{d}\tau \tag{1}$$

where ϕ_{ir} is the ith element in the rth mode shape; m_r, ζ_r and ω_{nr} are the modal mass, modal damping ratio and natural frequency of the rth mode, respectively; $\omega_{dr}=\omega_{nr}(1-\zeta_r^2)^{1/2}$ is the damped natural frequency of the rth mode; n is the number of modes; $g_r(t)$is the impulse response function related to modal parameters of the rth mode, i.e.

$$g_r(t)=\begin{cases}0, & t<0\\ \dfrac{\mathrm{e}^{-\zeta_r\omega_{nr}t}}{m_r\omega_{dr}}\sin(\omega_{dr}t), & t\geq 0\end{cases} \tag{2}$$

Then, the cross correlation function of responses x_i and x_j under the excitation f_k can be expressed as

$$R_{x_ix_jf_k}(T)=\sum_{r=1}^{n}\sum_{s=1}^{n}\phi_{ir}\phi_{kr}\phi_{js}\phi_{ks}\int_{-\infty}^{t}\int_{-\infty}^{t+T}g_r(t+T-\sigma)g_s(t-\tau)\mathrm{E}\{f_k(\sigma)f_k(\tau)\}\,\mathrm{d}\sigma\,\mathrm{d}\tau \tag{3}$$

where subscripts r and s indicate the rth and sth modal parameters, respectively; subscripts i, j and k indicate the ith, jth and kth measurement point, respectively.

If the excitation f_k is white noise, then

$$\mathrm{E}\{f_k(\tau)f_k(\sigma)\}=R_{f_kf_k}(\tau-\sigma)=\alpha_k\delta(\tau-\sigma) \tag{4}$$

where $2\alpha_k$ is a constant representing the one-side auto-spectral density of white noise, $\delta(t)$ is the Dirac Delta function. Then, substituting Eq. (4) into Eq. (3) and considering m excitations, the cross correlation function of responses x_i and x_j under m excitations can be simplified as

$$R_{x_ix_j}(T)=\sum_{r=1}^{n}\frac{\phi_{ir}G_{j,r}}{m_r\omega_{dr}}\mathrm{e}^{-\zeta_r\omega_{nr}T}\sin(\omega_{dr}T+\vartheta_r) \tag{5}$$

where $G_{j,r}$ is a coefficient dependent on the rth modal parameters and response measurement points j, ϑ_r is a phase dependent on the rth modal parameters. Eq. (5) is the fundamental formula of the NExT modal identification technique. Thus, modal identification techniques for impulse response functions can also be directly applied to the cross correlation functions between two responses under white noise excitation [24,25].

2.1.2. Definition of inner product vector

In principle, a damage detection procedure under white noise excitation might comprise: (1) identifying the modal parameters of the structure based on NExT; (2) utilizing the identified modal parameters to detect damage of the structure. However, identification errors inevitably occur in the modal identification procedure, which may influence the effectiveness of the damage detection methods. In order to avoid the effect of errors in modal identification on the damage detection procedure, the IPV was proposed in [23], and a generalised definition of the IPV is proposed in the following section.

When the time lag T=0, and considering the cross correlation function between all combinations of response measurement points 1,2, …, p, a $p\times p$ dimensional matrix can be obtained. For convenience, the Inner Product Vector is defined by one row (or column) of the $p\times p$ dimensional matrix, as follows:

$$\mathbf{R}_{\mathrm{IPV}}^{\mathrm{dis}}=[R_{x_1x_j}(0),R_{x_2x_j}(0),\ldots,R_{x_px_j}(0)]^{\mathrm{T}} \tag{6}$$

where $R_{x_ix_j}(0)=\sum_{r=1}^{n}(\phi_{ir}G_{j,r}\sin(\vartheta_r)/m_r\omega_{dr})=\sum_{r=1}^{n}\phi_{ir}\kappa_{j,r}^{\mathrm{dis}}$, $\kappa_{j,r}^{\mathrm{dis}}$ is a coefficient dependent on the rth modal parameters and the response measurement point j and the excitation positions, the superscript 'dis' indicates that the quantity is related to displacement, and x_j can be considered as the displacement response at the reference measurement point for the IPV. Then, the theoretical formula and calculating formula for the IPV can be obtained, respectively, as follows:

$$\mathbf{R}_{\mathrm{IPV}}^{\mathrm{dis}}=\sum_{r=1}^{n}\kappa_{j,r}^{\mathrm{dis}}[\phi_{1r},\phi_{2r},\ldots,\phi_{pr}]^{\mathrm{T}}=\sum_{r=1}^{n}\kappa_{j,r}^{\mathrm{dis}}\boldsymbol{\phi}_r \tag{7}$$

$$\mathbf{R}_{\mathrm{IPV}}^{\mathrm{dis}}=\frac{1}{N_s}[\langle\mathbf{x}_1,\mathbf{x}_j\rangle,\langle\mathbf{x}_2,\mathbf{x}_j\rangle,\ldots,\langle\mathbf{x}_p,\mathbf{x}_j\rangle]^{\mathrm{T}} \tag{8}$$

where $\boldsymbol{\phi}_r=[\phi_{1r},\phi_{2r},\ldots,\phi_{pr}]^{\mathrm{T}}$ is the rth mode shape, $\langle\mathbf{x},\mathbf{y}\rangle$ is the inner product of the two vectors $\mathbf{x}$ and $\mathbf{y}$, N_s is the length of $\mathbf{x}$ or $\mathbf{y}$. Therefore, the IPV is a weighted summation of the mode shapes of the structure, and the weighting factor of each mode shape only depends on the modal parameters of the structure. Meanwhile, the IPV can be directly calculated by the time domain vibration responses. As we know, changes in local physical parameters can induce abrupt changes in some mode shapes. Accordingly, the IPV of the damaged structure may also have abrupt changes. Thus, the IPV may be adopted as damage feature vector for structural damage detection.

2.1.3. Inner product vector defined by velocity or acceleration under white noise excitation

As the responses under white noise excitation are stationary stochastic process, the following equation is satisfied [26,27]:

$$\begin{gathered}R'_{x_i\dot{x}_j}(T)=R_{\dot{x}_i\dot{x}_j}(T)=-R_{x_i\ddot{x}_j}(T)\\ R''_{x_i\dot{x}_j}(T)=-R_{\dot{x}_i\ddot{x}_j}(T)\\ R''''_{x_i\dot{x}_j}(T)=R_{\ddot{x}_i\ddot{x}_j}(T)\end{gathered} \tag{9}$$

where $\dot{x}_i(t)=\mathrm{d}x_i(t)/\mathrm{d}t$ and $\ddot{x}_i(t)=\mathrm{d}^2x_i(t)/\mathrm{d}t^2$ are the velocity and acceleration response, respectively; $R_{\dot{x}_i\dot{x}_j}(T)$ and $R_{\ddot{x}_i\ddot{x}_j}(T)$ are cross correlation functions calculated by velocity and acceleration, respectively; $R'_{x_i\dot{x}_j}(T)=\mathrm{d}R_{x_i\dot{x}_j}(T)/\mathrm{d}T$, $R''_{x_i\dot{x}_j}(T)=\mathrm{d}^2R_{x_i\dot{x}_j}(T)/\mathrm{d}T^2$ and $R''''_{x_i\dot{x}_j}(T)=\mathrm{d}^4R_{x_i\dot{x}_j}(T)/\mathrm{d}T^4$ are the first-order, second-order and fourth-order derivatives of the cross correlation function $R_{x_ix_j}(T)$ with respect to changes in time lag T, respectively. Thus

$$R_{\dot{x}_i\dot{x}_j}(T)=-R''_{x_ix_j}(T)=\sum_{r=1}^{n}\frac{\phi_{ir}G_{j,r}}{m_r\omega_{dr}}\mathrm{e}^{-\zeta_r\omega_{nr}T}\left[-\zeta_r^2\omega_{nr}^2\sin(\omega_{dr}T+\vartheta_r)+2\zeta_r\omega_{nr}\omega_{dr}\cos(\omega_{dr}T+\vartheta_r)+\omega_{dr}^2\sin(\omega_{dr}T+\vartheta_r)\right] \tag{10}$$

$$\begin{aligned}R_{\ddot{x}_i\ddot{x}_j}(T)=R''''_{x_ix_j}(T)=\sum_{r=1}^{n}\frac{\phi_{ir}G_{j,r}}{m_r\omega_{dr}}\mathrm{e}^{-\zeta_r\omega_{nr}T}\Big[&\zeta_r^4\omega_{nr}^4\sin(\omega_{dr}T+\vartheta_r)-4\zeta_r^3\omega_{nr}^3\omega_{dr}\cos(\omega_{dr}T+\vartheta_r)-6\zeta_r^2\omega_{nr}^2\omega_{dr}^2\sin(\omega_{dr}T+\vartheta_r)\\&+4\zeta_r\omega_{nr}\omega_{dr}^3\cos(\omega_{dr}T+\vartheta_r)+\omega_{dr}^4\sin(\omega_{dr}T+\vartheta_r)\Big]\end{aligned} \tag{11}$$

Then, when time lag T=0

$$R_{\dot{x}_i\dot{x}_j}(0)=\sum_{r=1}^{n}\frac{\phi_{ir}G_{j,r}}{m_r\omega_{dr}}\left[-\zeta_r^2\omega_{nr}^2\sin(\vartheta_r)+2\zeta_r\omega_{nr}\omega_{dr}\cos(\vartheta_r)+\omega_{dr}^2\sin(\vartheta_r)\right]=\sum_{r=1}^{n}\phi_{ir}\kappa_{j,r}^{\mathrm{vel}} \tag{12}$$

$$R_{\ddot{x}_i\ddot{x}_j}(0)=\sum_{r=1}^{n}\frac{\phi_{ir}G_{j,r}}{m_r\omega_{dr}}\left[\zeta_r^4\omega_{nr}^4\sin(\vartheta_r)-4\zeta_r^3\omega_{nr}^3\omega_{dr}\cos(\vartheta_r)-6\zeta_r^2\omega_{nr}^2\omega_{dr}^2\sin(\vartheta_r)+4\zeta_r\omega_{nr}\omega_{dr}^3\cos(\vartheta_r)+\omega_{dr}^4\sin(\vartheta_r)\right]=\sum_{r=1}^{n}\phi_{ir}\kappa_{j,r}^{\mathrm{acc}} \tag{13}$$

where $\kappa_{j,r}^{\mathrm{vel}}$ and $\kappa_{j,r}^{\mathrm{acc}}$ are coefficients dependent on the rth modal parameters and the response measurement point j and the excitation positions, the superscript 'vel' or 'acc' indicate the quantity is related to velocity or acceleration, respectively.

Similar to Eq. (6), the IPVs $\mathbf{R}_{\mathrm{IPV}}^{\mathrm{vel}}$ and $\mathbf{R}_{\mathrm{IPV}}^{\mathrm{acc}}$, which are constructed by velocity and acceleration, respectively, are defined as

$$\mathbf{R}_{\mathrm{IPV}}^{\mathrm{vel}}=[R_{\dot{x}_1\dot{x}_j}(0),R_{\dot{x}_2\dot{x}_j}(0),\ldots,R_{\dot{x}_p\dot{x}_j}(0)]^{\mathrm{T}} \tag{14}$$

$$\mathbf{R}_{\mathrm{IPV}}^{\mathrm{acc}}=[R_{\ddot{x}_1\ddot{x}_j}(0),\ R_{\ddot{x}_2\ddot{x}_j}(0),\ \ldots,\ R_{\ddot{x}_p\ddot{x}_j}(0)]^{T} \tag{15}$$

Thus, the theoretical formula of IPVs of velocity and acceleration are

$$\mathbf{R}_{\mathrm{IPV}}^{\mathrm{vel}}=\sum_{r=1}^{n}\kappa_{j,r}^{\mathrm{vel}}[\phi_{1r},\ \phi_{2r},\ \ldots,\ \phi_{pr}]^{\mathrm{T}}=\sum_{r=1}^{n}\kappa_{j,r}^{\mathrm{vel}}\boldsymbol{\phi}_r \tag{16}$$

$$\mathbf{R}_{\mathrm{IPV}}^{\mathrm{acc}}=\sum_{r=1}^{n}\kappa_{j,r}^{\mathrm{acc}}[\phi_{1r},\ \phi_{2r},\ \ldots,\ \phi_{pr}]^{\mathrm{T}}=\sum_{r=1}^{n}\kappa_{j,r}^{\mathrm{acc}}\boldsymbol{\phi}_r \tag{17}$$

The IPVs $\mathbf{R}_{\mathrm{IPV}}^{\mathrm{vel}}$ and $\mathbf{R}_{\mathrm{IPV}}^{\mathrm{acc}}$ can be calculated by

$$\mathbf{R}_{\mathrm{IPV}}^{\mathrm{vel}} = \frac{1}{N_s}[\langle \dot{\mathbf{x}}_1, \dot{\mathbf{x}}_j \rangle, \langle \dot{\mathbf{x}}_2, \dot{\mathbf{x}}_j \rangle, \ldots, \langle \dot{\mathbf{x}}_p, \dot{\mathbf{x}}_j \rangle]^{\mathrm{T}} \tag{18}$$

$$\mathbf{R}_{\mathrm{IPV}}^{\mathrm{acc}} = \frac{1}{N_s}[\langle \ddot{\mathbf{x}}_1, \ddot{\mathbf{x}}_j \rangle, \langle \ddot{\mathbf{x}}_2, \ddot{\mathbf{x}}_j \rangle, \ldots, \langle \ddot{\mathbf{x}}_p, \ddot{\mathbf{x}}_j \rangle]^{\mathrm{T}} \tag{19}$$

Similar to the IPV defined by displacement, the IPV defined by velocity or acceleration may be adopted as a damage feature vector for structural damage detection as well.

2.2. Inner product vector under band pass white noise excitation

In the above section, the theoretical formulae (7), (16) and (17) for IPVs are deduced based on the assumption that the excitations are white noise. Unfortunately, the ideal white noise with unlimited bandwidth is inexistent in practice. Usually, band pass white noise (i.e. bandwidth limited white noise) is utilized instead. Therefore, IPVs under band pass white noise excitation are investigated in this section.

If the bandwidth of the white noise is limited, the auto correlation function of white noise in Eq. (4) should be changed to the auto correlation function of band pass white noise, which is given by [26]

$$R_{f_i f_k}(\tau-\sigma) = \mathrm{E}\{f_k(\tau) f_k(\sigma)\} = \alpha_k C_k \left(\frac{\sin(\pi C_k(\tau-\sigma))}{\pi C_k(\tau-\sigma)} \cos(2\pi C_{k,c}(\tau-\sigma)) \right) \tag{20}$$

where the constant α_k is the one-side auto-spectral density of the band pass white noise, C_k is the bandwidth and $C_{k,c}$ is central frequency. Substituting Eq. (20) into Eq. (3), one obtains

$$R_{x_i x_j f_k}(T) = \sum_{r=1}^{n}\sum_{s=1}^{n} \phi_{ir}\phi_{kr}\phi_{js}\phi_{ks} \int_{-\infty}^{t}\int_{-\infty}^{t+T} \alpha_k C_k g_r(t+T-\sigma) g_s(t-\tau) \frac{\sin(\pi C_k(\tau-\sigma))}{\pi C_k(\tau-\sigma)} \cos(2\pi C_{k,c}(\tau-\sigma)) \,\mathrm{d}\sigma \,\mathrm{d}\tau \tag{21}$$

Changing the variables of integration by letting $t-\sigma=\lambda_1$, $t-\tau=\lambda_2$, Eq. (21) becomes

$$R_{x_i x_j f_k}(T) = \sum_{r=1}^{n}\sum_{s=1}^{n} \phi_{ir}\phi_{kr}\phi_{js}\phi_{ks} \int_{0}^{+\infty}\int_{-T}^{+\infty} \alpha_k C_k g_r(T+\lambda_1) g_s(\lambda_2) \frac{\sin(\pi C_k(\lambda_1-\lambda_2))}{\pi C_k(\lambda_1-\lambda_2)} \cos(2\pi C_{k,c}(\lambda_1-\lambda_2)) \,\mathrm{d}\lambda_1 \,\mathrm{d}\lambda_2 \tag{22}$$

Though the terms involving T can be separated from those involving λ_1 by the definition of $g_r(T+\lambda_1)$ [24], the lower limit of the inner integration is a function of T. Thus, it is impossible to separate the variable T from the integration, i.e. Eq. (22) cannot be simplified in the form of Eq. (5). Fortunately, as the IPV is defined by the cross correlation when time lag $T=0$, only the cross correlation functions at time lag $T=0$ need to be discussed. Meanwhile, as it is impossible to obtain an analytical formula for $R_{x_i x_j}(T)$ in the form of Eq. (5), IPVs of velocity and acceleration cannot be deduced by the definition of IPV of displacement through Eq. (9). Therefore, under band pass white noise excitation, IPVs defined by displacement, velocity and acceleration are discussed.

2.2.1. Inner product vector defined by displacement

Substituting $T=0$ and Eq. (2) into Eq. (22)

$$\begin{aligned} R_{x_i x_j f_k}(0) = \sum_{r=1}^{n}\sum_{s=1}^{n} \frac{\phi_{ir}\phi_{kr}\phi_{js}\phi_{ks}}{m_r\omega_{dr}m_s\omega_{ds}} \int_{0}^{+\infty}\int_{0}^{+\infty} \alpha_k C_k \mathrm{e}^{-\zeta_r\omega_{nr}\lambda_1-\zeta_s\omega_{ns}\lambda_2} \sin(\omega_{dr}\lambda_1)\sin(\omega_{dr}\lambda_2) \\ \times \frac{\sin(2\pi C_k(\lambda_1-\lambda_2))\cos(2\pi C_{k,c}(\lambda_1-\lambda_2))}{2\pi C_k(\lambda_1-\lambda_2)} \,\mathrm{d}\lambda_1 \,\mathrm{d}\lambda_2 \end{aligned} \tag{23}$$

It is easily verified that the double integration in the above equation is convergent; thus

$$R_{x_i x_j f_k}(0) = \sum_{r=1}^{n}\sum_{s=1}^{n} \frac{\phi_{ir}\phi_{kr}\phi_{js}\phi_{ks}}{m_r\omega_{dr}m_s\omega_{ds}} \beta_{k,rs}^{\mathrm{dis}} \tag{24}$$

where $\beta_{k,rs}^{\mathrm{dis}}$ is the value of the double integration, which is dependent on the rth and sth modal parameters, the one-side auto-spectral density α_k, bandwidth C_k and central frequency $C_{k,c}$ of the band pass white noise.

Thus, the cross correlation function due to m excitations is expressed as

$$R_{x_i x_j}(0) = \sum_{r=1}^{n}\sum_{s=1}^{n}\sum_{k=1}^{m} \frac{\beta_{k,rs}^{\mathrm{dis}}\phi_{ir}\phi_{kr}\phi_{js}\phi_{ks}}{m_r\omega_{dr}m_s\omega_{ds}} = \sum_{r=1}^{n} \phi_{ir}\zeta_{j,r}^{\mathrm{dis}} \tag{25}$$

where $\zeta_{j,r}^{\mathrm{dis}} = \sum_{s=1}^{n}\sum_{k=1}^{m} \frac{\beta_{k,rs}^{\mathrm{dis}}\phi_{kr}\phi_{js}\phi_{ks}}{m_r\omega_{dr}m_s\omega_{ds}}$ is the weighting factor of the rth mode shape, which is dependent on the reference response measurement point j, the rth modal parameters (including natural frequency, mode shape, modal damping and modal mass), and all the band pass white noise excitations (including the number of excitations, the position of each excitation, and their auto-spectral density, bandwidth and central frequency). Then substituting Eq. (25) to Eq. (6), the theoretical formula for the IPV calculated from displacements under band pass white noise excitation can be achieved.

2.2.2. Inner product vector defined by velocity or acceleration

Similar to displacement and assuming zero initial conditions, the velocity $\dot{x}_{ik}(t)$ and acceleration $\ddot{x}_{ik}(t)$ at point i due to a single excitation $f_k(t)$ at point k are

$$\dot{x}_{ik}(t) = \sum_{r=1}^{n} \phi_{ir}\phi_{kr} \int_{-\infty}^{t} f_k(\tau)\dot{g}_r(t-\tau)\,\mathrm{d}\tau \tag{26}$$

$$\ddot{x}_{ik}(t) = \sum_{r=1}^{n} \phi_{ir}\phi_{kr} \int_{-\infty}^{t} f_r(\tau)\ddot{g}_r(t-\tau)\,\mathrm{d}\tau \tag{27}$$

where

$$\dot{g}_r(t) = \frac{\mathrm{d}}{\mathrm{d}t}[g_r(t)] = \begin{cases} 0, & t<0 \\ \dfrac{\mathrm{e}^{-\zeta_r\omega_{nr}t}}{m_r\omega_{dr}}\left[-\zeta_r\omega_{nr}\sin(\omega_{dr}t)+\omega_{dr}\cos(\omega_{dr}t)\right], & t\geq 0 \end{cases} \tag{28}$$

$$\ddot{g}_r(t) = \frac{\mathrm{d}^2}{\mathrm{d}t^2}[g_r(t)] = \begin{cases} 0, & t<0 \\ \dfrac{\mathrm{e}^{-\zeta_r\omega_{nr}t}}{m_r\omega_{dr}}\left[\zeta_r^2\omega_{nr}^2\sin(\omega_{dr}t)-2\zeta_r\omega_{nr}\omega_{dr}\cos(\omega_{dr}t)-\omega_{dr}^2\sin(\omega_{dr}t)\right], & t\geq 0 \end{cases} \tag{29}$$

Then, using the same procedure as the deduction for displacement IPV, the cross correlation functions of velocities and accelerations due to m excitations are expressed as

$$R_{\dot{x}_i\dot{x}_j}(0) = \sum_{r=1}^{n}\sum_{s=1}^{n}\sum_{k=1}^{m} \frac{\beta_{k,rs}^{\mathrm{vel}}\phi_{ir}\phi_{kr}\phi_{js}\phi_{ks}}{m_r\omega_{dr}m_s\omega_{ds}} = \sum_{r=1}^{n} \phi_{ir}\zeta_{j,r}^{\mathrm{vel}} \tag{30}$$

$$R_{\ddot{x}_i\ddot{x}_j}(0) = \sum_{r=1}^{n}\sum_{s=1}^{n}\sum_{k=1}^{m} \frac{\beta_{k,rs}^{\mathrm{acc}}\phi_{ir}\phi_{kr}\phi_{js}\phi_{ks}}{m_r\omega_{dr}m_s\omega_{ds}} = \sum_{r=1}^{n} \phi_{ir}\zeta_{j,r}^{\mathrm{acc}} \tag{31}$$

where $\beta_{k,rs}^{\mathrm{vel}}$ and $\beta_{k,rs}^{\mathrm{acc}}$ are coefficients dependent on the rth and sth modal parameters, the one-side auto-spectral density α_k, bandwidth C_k and central frequency $C_{k,c}$ of the band bass white noise; $\zeta_{j,r}^{\mathrm{vel}} = \sum_{s=1}^{n}\sum_{k=1}^{m}(\beta_{k,rs}^{\mathrm{vel}}\phi_{kr}\phi_{js}\phi_{ks}/m_r\omega_{dr}m_s\omega_{ds})$ and $\zeta_{j,r}^{\mathrm{acc}} = \sum_{s=1}^{n}\sum_{k=1}^{m}(\beta_{k,rs}^{\mathrm{acc}}\phi_{kr}\phi_{js}\phi_{ks}/m_r\omega_{dr}m_s\omega_{ds})$ are the weighting factors of the rth mode shape, which is dependent on the reference response measurement point j, the rth modal parameters (including natural frequency, mode shape, modal damping and modal mass) and all the band pass white noise excitations (including the number of excitations, the position of each excitation, and their auto-spectral density, bandwidth and central frequency). Then, the theoretical formula for the IPV calculated from velocities or accelerations under band pass white noise excitation can be achieved by utilizing Eq. (30) instead of Eq. (12) or utilizing Eq. (31) instead of Eq. (13).

2.3. Influence of measurement noise on inner product vector

Based on the definition of IPV in this paper, it is easy to verify the robustness of the IPV to noise using the same procedure as our previous research [23]. It can be concluded that: (1) the point inner product in the IPV is polluted by the measurement noise and (2) the cross inner product in the IPV is unpolluted by the measurement noise. However, it should be mentioned that the measurement noise should satisfy the following assumptions: (1) the measurement noise has zero mean; (2) the measurement noise is independent of the vibration response without measurement noise; (3) the measurement noise of different measurement points is independent of each other.

As the measurement noise does not satisfy the above three assumptions well, both the cross inner product and point inner product will be polluted by measurement noise, but the effect on the point inner product is more severe. Two potential methods may be adopted to deal with the effect of measurement noise on the point inner product: (1) when the measurement noise level is not serious, and the measurement noise level is unchanged in the measurement of intact and damaged structures, a damage index defined by the difference between the IPVs of the intact and damaged structures can be utilized to decrease the effect of measurement noise (i.e. the method selected in this paper, see Section 3.1); (2) the point inner product can be discarded in the inner product vector, i.e., the response at the reference measurement point is merely a reference, and its point inner product is not utilized in the damage detection procedure.

3. Structural damage detection method based on inner product vector

3.1. Definition of damage index

Local damage in the structure can induce changes in local physical parameters (such as mass or stiffness) of the structure, as well as abrupt changes in local mode shapes. Accordingly, the IPV of the damaged structure may exhibit

abrupt changes. However, changes in physical parameters of the damaged structure are usually rather small in the initial stage of damage detection, so changes in the IPV of a damaged structure will be smooth and cannot be distinguished clearly. Thus, the damage index can be formulated by the changes between the IPVs of the intact and damaged structures. In theoretical formulae of the IPVs, there is a multiplying constant α_k referring to the auto-spectral density of the band pass white noise excitation. In order to eliminate the influence of the auto-spectral density of the white noise excitation, the IPV should be normalized at first. In the current research, the $\mathbf{R}_{\mathrm{IPV}}$ is normalized by its root mean square value

$$\overline{\mathbf{R}}_{\mathrm{IPV}} = \frac{\mathbf{R}_{\mathrm{IPV}}}{\mathrm{RMS}(\mathbf{R}_{\mathrm{IPV}})} \tag{32}$$

For the sake of convenience, the normalized IPV is still denoted by the symbol $\mathbf{R}_{\mathrm{IPV}}$ in the following sections. Then, the local damage index can be formulated as

$$D_{\mathrm{IPV},i} = R^d_{\mathrm{IPV},i} - R^u_{\mathrm{IPV},i} \tag{33}$$

where $R^u_{\mathrm{IPV},i}$ and $R^d_{\mathrm{IPV},i}$ indicate the ith element in the IPVs of the intact and damage structures, respectively. Thus, the damage index is defined as $\mathbf{D}_{\mathrm{IPV}} = \{D_{\mathrm{IPV},1}, D_{\mathrm{IPV},2}, \ldots, D_{\mathrm{IPV},N_m}\}$. Supposing that the noise level of the same measurement point is unchanged in the intact and damaged structure, the values of point inner products of the intact and damaged structure are approximately polluted by the same value according to the variance of the measurement noise, respectively. Thus, the absolute change in point inner products of the intact and damaged structures is of benefit to decrease the effect of measurement noise on the damage index $\mathbf{D}_{\mathrm{IPV}}$. Therefore, the damage index formulated by Eq. (33) improves the robustness of the IPV-based structural damage detection method to noise, and the damage might be located by abrupt changes in $\mathbf{D}_{\mathrm{IPV}}$. In order to utilize the local maximum of the damage index to locate the damage, three different types of abrupt changes in $\mathbf{D}_{\mathrm{IPV}}$ should be considered, as follows.

If the abrupt change is an "impulse change" (see Fig. 1(a)), the damage location of the structure is in the vicinity of the measurement point corresponding to the local maximum of $\mathbf{D}_{\mathrm{IPV}}$.

If the abrupt change is a "step change" (see Fig. 1(b)), the first-order difference of $\mathbf{D}_{\mathrm{IPV}}$ is utilized as the damage index, which is defined by

$$D'_{\mathrm{IPV},i+0.5} = D_{\mathrm{IPV},i+1} - D_{\mathrm{IPV},i} \tag{34}$$

where $i = 1, 2, \ldots, N_m - 1$, N_m is the number of elements in $\mathbf{D}_{\mathrm{IPV}}$. The abrupt changes in $\mathbf{D}_{\mathrm{IPV}}$ correspond to the local maximum of $\mathbf{D}'_{\mathrm{IPV}}$. Then, if the local maximum of $\mathbf{D}'_{\mathrm{IPV}}$ occurs in $i+0.5$, the damage is located between the measurement point i and $i+1$.

If the abrupt change is a "weak impulse change" (see Fig. 1(c)), the second-order difference of $\mathbf{D}_{\mathrm{IPV}}$ is utilized as the damage index, which is defined by

$$D''_{\mathrm{IPV},i+1} = D_{\mathrm{IPV},i+2} - 2D_{\mathrm{IPV},i+1} + D_{\mathrm{IPV},i} \tag{35}$$

where $i = 1,2, \ldots, N_m - 2$. The abrupt changes in $\mathbf{D}_{\mathrm{IPV}}$ correspond to the local maximum of $\mathbf{D}''_{\mathrm{IPV}}$. Then, if the local maximum of $\mathbf{D}''_{\mathrm{IPV}}$ occurs in $i+1$ the damage is located in the vicinity of the measurement point $i+1$.

It should be emphasized that the abrupt changes in $\mathbf{D}_{\mathrm{IPV}}$ can be directly utilized to locate the damage irrespective of the abrupt changes in $\mathbf{D}_{\mathrm{IPV}}$ being "impulse change", or "step change" or "weak impulse change". However, in order to locate the damage more clearly and propose an automatic detection procedure, the first- or second-order difference can be performed on $\mathbf{D}_{\mathrm{IPV}}$. And then, the local maximum of $\mathbf{D}_{\mathrm{IPV}}$ or $\mathbf{D}'_{\mathrm{IPV}}$ or $\mathbf{D}''_{\mathrm{IPV}}$ can be utilized to locate the damage.

After the damage is located by the abrupt changes in $\mathbf{D}_{\mathrm{IPV}}$, the damage extent may be evaluated by the extent of the abrupt changes in $\mathbf{D}_{\mathrm{IPV}}$. However, the relations between abrupt changes in $\mathbf{D}_{\mathrm{IPV}}$ and damage extent are rather complex, and the relations should be different for different models. Meanwhile, the main purpose of the proposed method is merely to locate the damage. Therefore, the detection of damage extent is not considered in this research.

3.2. Threshold for damage detection

Many damage detection methods, especially the methods in which damage is detected by the local maximum of the damage index, refer to a threshold for classifying the damaged and intact structure. Some investigations, such as Wang and Ren [20], Trendafilova and Manoach [22], Kim and Stubbs [28], showed good results even though the thresholds were not

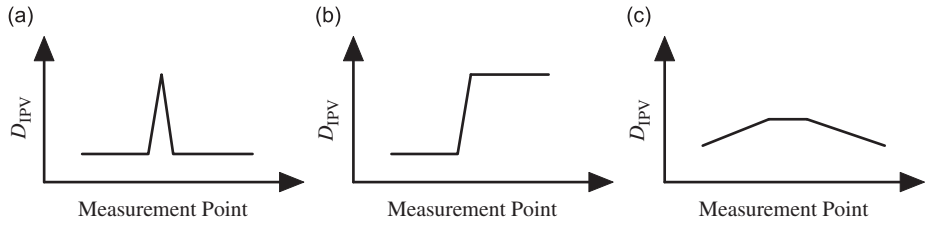

Fig. 1. The types of abrupt changes in $\mathbf{D}_{\mathrm{IPV}}$: (a) impulse change, (b) step change and (c) weak impulse change.

defined. However, it may be difficult to distinguish the local maximum caused by local damage and various errors. In conclusion, choosing the threshold should be a critical problem for utilizing such methods in practice.

The IPV-based structural damage detection method proposed in this paper is one such method in which the damage is detected by the local maximum of the damage index. Local maxima in $\mathbf{D}_{\mathrm{IPV}}$ (or $\mathbf{D}'_{\mathrm{IPV}}$ or $\mathbf{D}''_{\mathrm{IPV}}$) can arise due to local damage, but also due to various errors, such as measurement noise and assumptions of the excitations. Therefore, a threshold is needed to distinguish a local maximum caused by local damage and various errors.

Different methods for ascertaining the threshold were proposed by many researchers for their methods. For example, in the damage detection method based on outlier analysis, Worden et al. [17] assumed that the observation vectors of the intact structure are normally distributed, and used Monte Carlo simulation to define a threshold that is just dependent on the number and dimension of the observation vectors. In the investigation of Yan et al. [29], they also assumed that the measurement data of the intact structure are normally distributed, and based on the mean value and standard deviation of the measurement data, the threshold was defined by the 3σ criterion. In the investigation of Alvandi and Cremona [14] and Choi et al. [15], the statistical pattern recognition based on the Neyman–Pearson criterion was adopted to classify the damaged and intact structure, and then the threshold was defined for different confidence levels.

The fundamental assumptions for defining the thresholds in the above researches were that the measurement data of the intact structure are normally distributed. Then, the measurement data of the damaged structure can be distinguished as outliers based on the threshold for the particular confidence level. The method adopted in this research is similar to that in reference [29], i.e. for a particular confidence interval, the upper threshold t_h and lower threshold t_l are defined by the mean value and standard deviation of $\mathbf{D}_{\mathrm{IPV}}$ (or $\mathbf{D}'_{\mathrm{IPV}}$ or $\mathbf{D}''_{\mathrm{IPV}}$), as follows:

$$t_h = \mu_D + \alpha_c \sigma_D$$
$$t_l = \mu_D - \alpha_c \sigma_D \tag{36}$$

where μ_D and σ_D are the mean value and standard deviation of $\mathbf{D}_{\mathrm{IPV}}$ (or $\mathbf{D}'_{\mathrm{IPV}}$ or $\mathbf{D}''_{\mathrm{IPV}}$), respectively, and α_c is a coefficient corresponding to a confidence interval, for example α_c=1.5 corresponds to a confidence interval of 86.64% with the assumption of a normal distribution. When the elements of $\mathbf{D}_{\mathrm{IPV}}$ (or $\mathbf{D}'_{\mathrm{IPV}}$ or $\mathbf{D}''_{\mathrm{IPV}}$) fall in the region between t_l and t_h, the structure is judged to be intact; otherwise, the structure is damaged.

Based on the above analysis, the procedure for utilizing the IPV-based structural damage detection method should be as follows:

Step 1: acquire time domain vibration responses of each measurement point of the intact structure under band pass white noise excitation;
Step 2: acquire time domain vibration responses of the current structure under the similar experimental condition as the test for the intact structure.
Step 3: calculate IPVs of the intact and current structures and the damage index $\mathbf{D}_{\mathrm{IPV}}$, and then choose $\mathbf{D}_{\mathrm{IPV}}$ or $\mathbf{D}'_{\mathrm{IPV}}$ or $\mathbf{D}''_{\mathrm{IPV}}$ as the damage index based on the type of the abrupt changes in $\mathbf{D}_{\mathrm{IPV}}$.
Step 4: set the confidence interval factor α_c and define the threshold, and then locate the damage by the local maximum of the damage index, which is beyond the threshold.

4. Experimental validations

As the IPV-based structural damage detection method was verified in our previous research by simulative examples [23], three experimental damage detection examples were performed in the current research, i.e. stiffness reduction detection of shear frame structure, debonding damage detection of honeycomb sandwich composite beam and bolt loosening detection of aircraft stiffened panel. As the accelerations are much easier to be acquired simultaneously in the experiment, we utilize the accelerations in the following experimental examples.

4.1. Shear frame structure

The 8-storey shear frame structure is shown in Fig. 2. There are 4 braces between each two floors, and each brace consists of 3 steel columns (the dimension of each column is 139 mm × 27 mm × 1 mm), i.e. there are 12 steel columns between each two floors. The stiffness of the frame in the y direction is much higher than the stiffness in the x direction, and only the vibration in the x direction is considered. In the experiment, the structure is excited at the first floor, and 8 accelerometers are affixed at each floor (as shown in Fig. 2). The local damage that occurred in the structure can be easily simulated by removing the steel column(s) between two floors; for example, the local damage extent (reduction of local stiffness) is approximately 1/12 corresponding to removing one steel column between two floors. And then 9 different damage cases are simulated in our experiment. Including the intact structure (which is utilized to illustrate that the IPV-based structural damage detection method can be utilized to distinguish the damaged and intact structures), 10 structural states are adopted as the current states to be detected, as listed in Table 1.

The first two natural frequencies of the intact structure can be easily measured by the sweep sine method, and they are 2.35 and 7.09 Hz. The accelerations of the intact structure and each simulated structure states are measured under 0–5 Hz

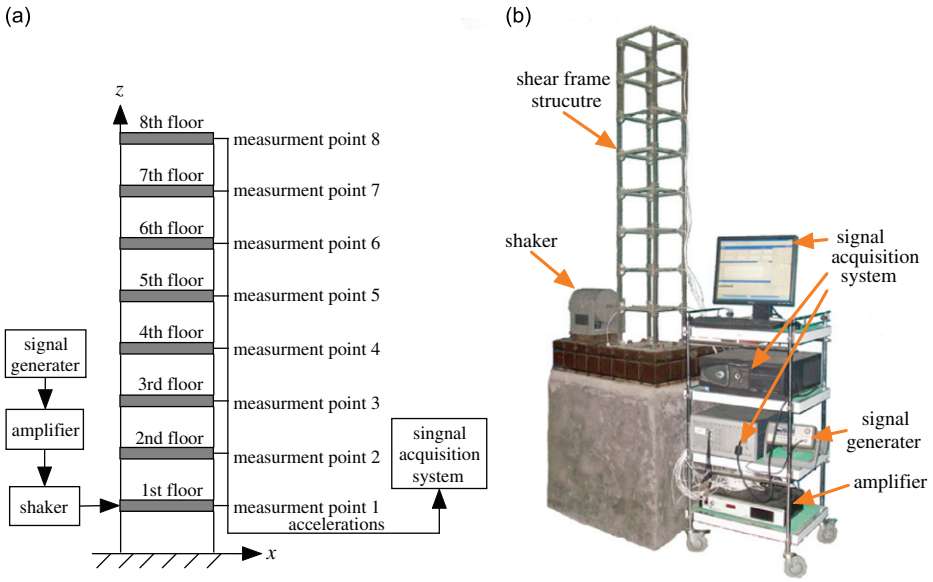

Fig. 2. 8-storey shear frame structure and the test setup: (a) sketch of test setup and (b) test setup.

Table 1
Simulated structure states of the 8-storey shear frame.

Structure state	D31	D32	D33	D51	D52	D53	D71	D72	D73	Intact
Damage location	Between 2nd floor and 3rd floor			Between 4th floor and 5th floor			Between 6th floor and 7th floor			None
Damage extent (stiffness reduction)	1/12	2/12	3/12	1/12	2/12	3/12	1/12	2/12	3/12	None

(which covers the fundamental natural frequency of the structure) band pass white noise excitations, and then the IPVs and the corresponding damage index are calculated, finally the damage in each simulated structure state is located. In the experiment, the reference response measurement point for calculating IPVs is the measurement point at the 8th floor (i.e. measurement point 8). Meanwhile, it is found that the abrupt changes in $\mathbf{D}_{\mathrm{IPV}}$ of the shear frame structure is "step change"; thus the local maximum of $\mathbf{D}'_{\mathrm{IPV}}$ is utilized to locate the damage, and the confidence interval factor α_c is set as 1.5 or 1.8.

Figs. 3–11 show the damage detection results of structure states D31, D32, D33, D51, D52, D53, D71, D72 and D73 of the shear frame structure. All the damage cases are correctly detected by the IPV-based structural damage detection method using the confidence interval factor α_c as 1.5 or 1.8, except that false negative detection occurred in structure state D71 (see Fig. 9). The reason for the false negative detection occurred in structure state D71 is that the effect of local damage simulated in structure state D71 on the lower modes is slight as the damage location is far from the base, i.e. structure state D71 is very close to the intact structure. Meanwhile, as the damage index $\mathbf{D}'_{\mathrm{IPV}}$ increases with the increase of the damage extent for the structure state with the same damage location and different damage extent, the damage extent might be qualitatively evaluated by the IPV-based structural damage detection method.

In order to illustrate that the IPV-based structural damage detection method can also be utilized to distinguish the damaged and intact structures, Fig. 12 shows the damage detection results of the intact structure (i.e. structure state Intact). It is clearly shown in Fig. 12 that the structure is undamaged using the confidence interval factor α_c as 1.5 or 1.8. Meanwhile, comparing the detection results of structure state D71 (Fig. 9, false negative detection occurred) and Intact (Fig. 12), the damage index $\mathbf{D}'_{\mathrm{IPV}}$ of the Intact state is much smaller than that of structure state D71. Thus, it can be inferred that the damage simulated in structure state D71 can be located if the confidence interval factor α_c is reduced. However, false positive detection might have occurred in some structure states due to the reduction the confidence interval factor α_c.

In conclusion, using the acceleration responses under 0–5 Hz band pass white noise excitation and setting the confidence interval factor α_c as 1.5 or 1.8, the IPV-based structural damage detection method can be utilized to correctly locate the damage location in the 8-storey shear frame structure if the damage extent is not very small, and distinguish the damaged and intact structures, as well as qualitatively evaluate the damage extent.

4.2. *Honeycomb sandwich composite beam*

Honeycomb sandwich composite structures are widely utilized in structural engineering. Unfortunately they are apt to suffer debonding damage when they are subjected to low energy impact in service. As it is usually impossible to detect the

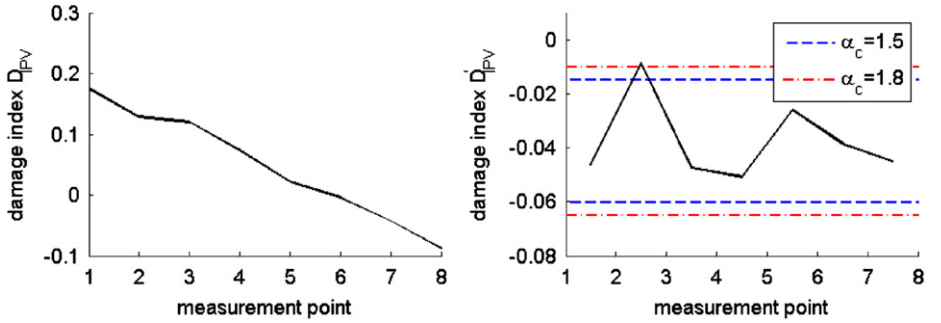

Fig. 3. Damage detection results of structure state D31 (the stiffness between 2nd floor and 3rd floor is reduced by 1/12).

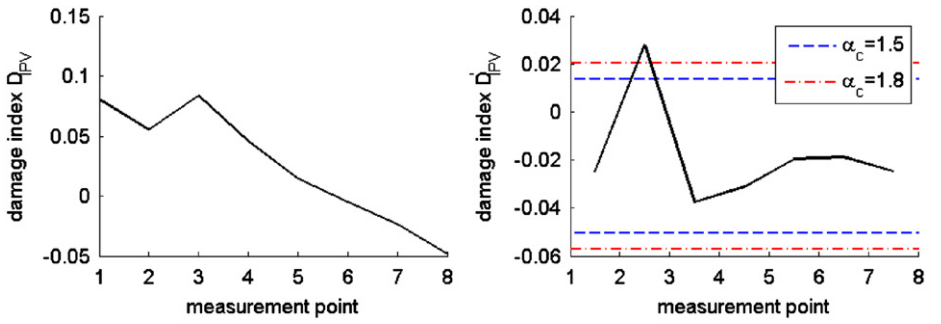

Fig. 4. Damage detection results of structure state D32 (the stiffness between 2nd floor and 3rd floor is reduced by 2/12).

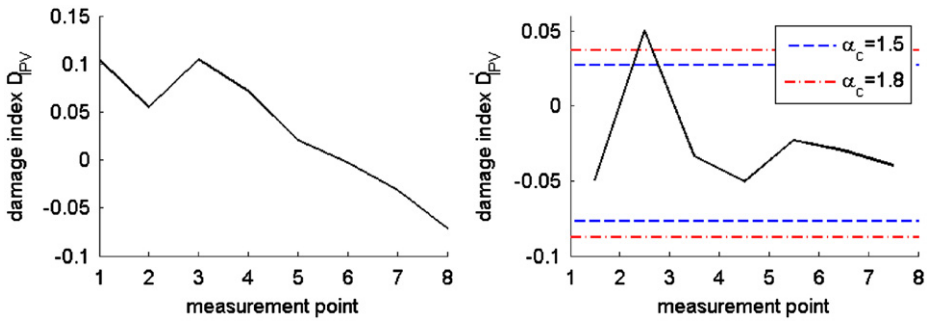

Fig. 5. Damage detection results of structure state D33 (the stiffness between 2nd floor and 3rd floor is reduced by 3/12).

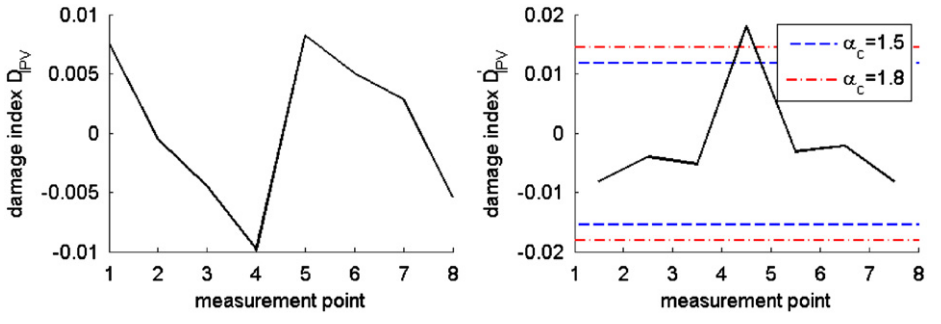

Fig. 6. Damage detection results of structure state D51 (the stiffness between 4th floor and 5th floor is reduced by 1/12).

debonding damage by visual inspection, the detection of the debonding damage becomes an important issue for these structures. In this section, the IPV-based structural damage detection method is adopted to detect the debonding damage of honeycomb sandwich composite beam.

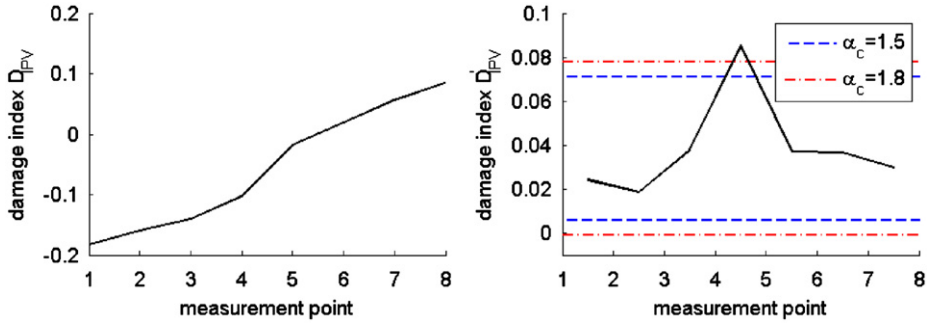

Fig. 7. Damage detection results of structure state D52 (the stiffness between 4th floor and 5th floor is reduced by 2/12).

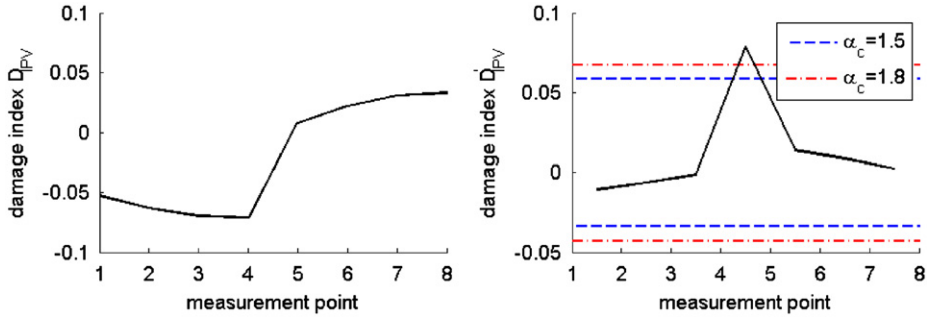

Fig. 8. Damage detection results of structure state D53 (the stiffness between 4th floor and 5th floor is reduced by 3/12).

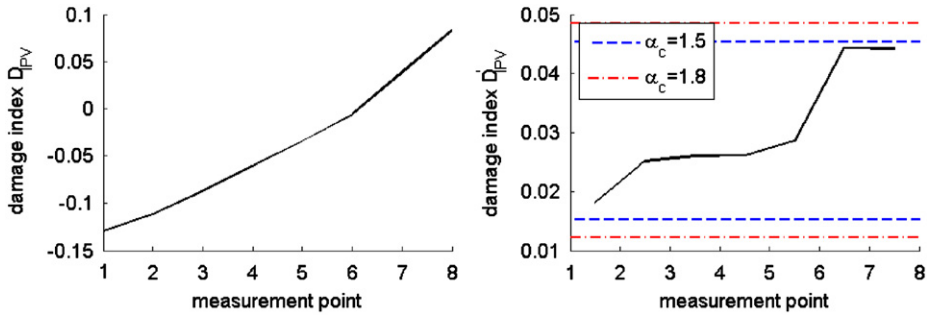

Fig. 9. Damage detection results of structure state D71 (the stiffness between 6th floor and 7th floor is reduced by 1/12).

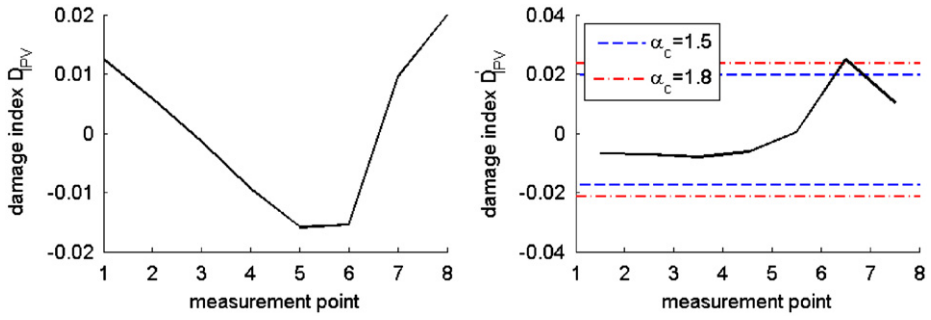

Fig. 10. Damage detection results of structure state D72 (the stiffness between 6th floor and 7th floor is reduced by 2/12).

The dimension of the honeycomb sandwich composite beam is 400 mm × 40 mm × 16 mm, as shown in Fig. 13. The core is made of hexagon aluminum honeycomb, and the surface panel is made of carbon fiber composite laminate panel. In the experiment, the honeycomb sandwich composite beam is excited by a noncontacted electromagnetic shaker at the free

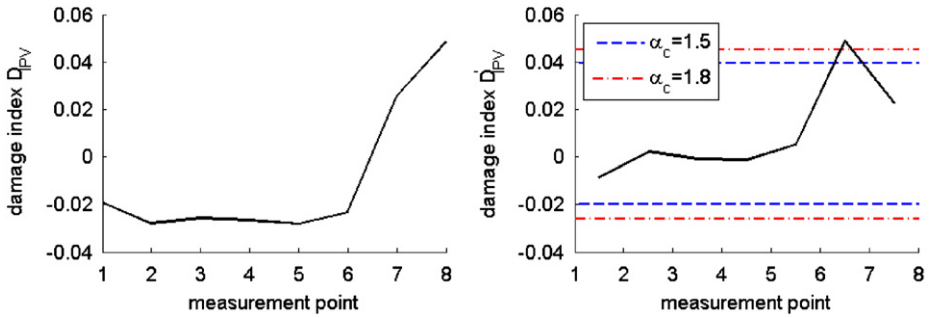

Fig. 11. Damage detection results of structure state D73 (the stiffness between 6th floor and 7th floor is reduced by 3/12).

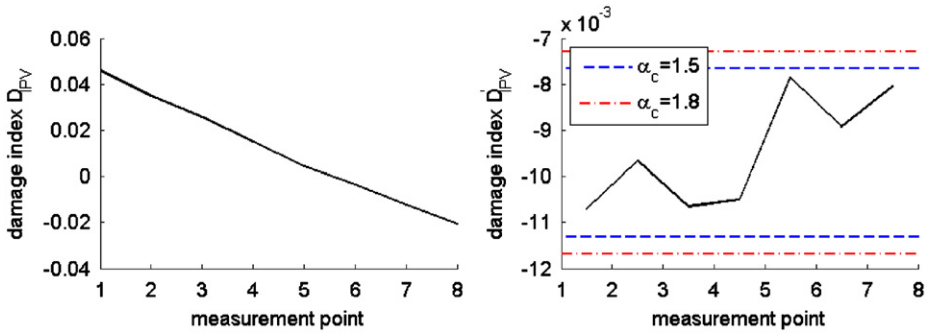

Fig. 12. Damage detection results of structure state Intact.

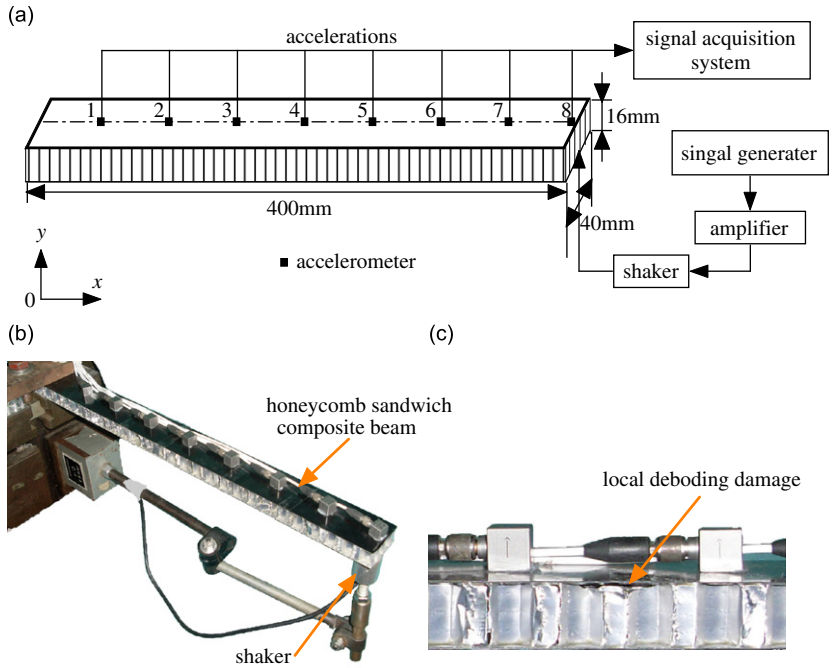

Fig. 13. Honeycomb sandwich composite beams and test setup: (a) sketch of test setup, (b) test setup and (c) deboding damage.

end of the beam, and 8 accelerometers are affixed along the beam with identical interval, i.e. the 8 accelerometers are affixed at 50, 150, …, 350 and 400 mm, respectively, as shown in Fig. 13. Using three identical honeycomb sandwich composite beams, artificial debonding damage is simulated at three different locations, respectively, as listed in Table 2.

The first two natural frequencies of the intact beam (Model 1) can be easily measured by sweep sine method, and they are 56.97 and 350.91 Hz. The accelerations of the intact structure and each simulated structure states are measured under 0–100 Hz (which covers the fundamental natural frequency of the structure) band pass white noise excitations, and then the IPVs and the corresponding damage index are calculated; finally the damage in each simulated structure state is located. In the experiment, the reference response measurement point for calculating IPVs is the measurement point at the free end of the beam (i.e. measurement point 8). Meanwhile, it is found that the abrupt change in $\mathbf{D}_{IPV}$ of honeycomb sandwich composite beam is "step change"; thus the local maximum of $\mathbf{D}'_{IPV}$ is utilized to locate the damage, and the confidence interval factor α_c is set as 1.5 or 1.8.

Figs. 14–16 show the damage detection results of structure states D11, D21 and D31 of the honeycomb sandwich composite beams. As shown in these figures, all the structure states of the honeycomb sandwich composite beams are correctly detected by the IPV-based structural damage detection method using the confidence interval factor α_c as 1.5 or 1.8. In conclusion, using the acceleration responses under 0–100 Hz band pass white noise excitation and setting the confidence interval factor α_c as 1.5 or 1.8, the IPV-based structural damage detection method can be utilized to correctly locate the debonding damage location in the honeycomb sandwich composite beams.

4.3. Aircraft stiffened panel

Stiffened panels are widely utilized in aeronautic structures in order to maximise the strength to weight ratio; however, damage occurring on the interface between the stringers and the panel, such as corrosion or loosening at the rivets, will significantly affect the performance of the structures. In this section, the IPV-based structural damage detection method is adopted to detect the damage occurring on the interface between the stringers and the panel.

The aircraft stiffened panel model is shown in Fig. 17. Both the panel and the stringers are made of aluminum, and the dimension of the panel is 750 mm × 35 mm × 0.5 mm. In order to simulate the intact and damage states of the structure more quickly and conveniently, bolts are utilized to replace the rivets in the experimental model, and the damage

Table 2
Simulated structure states of the honeycomb sandwich composite beams.

Structure state	D11	D21	D31
Experimental model	Model 1	Model 2	Model 3
Debonding location	Between 100 and 150 mm	Between 200 and 250 mm	Between 300 and 350 mm

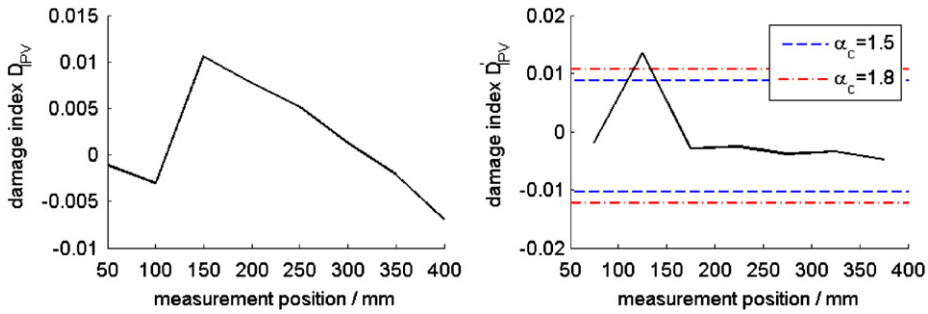

Fig. 14. Damage detection results of structure state D11 (debonding location is between 100 and 150 mm).

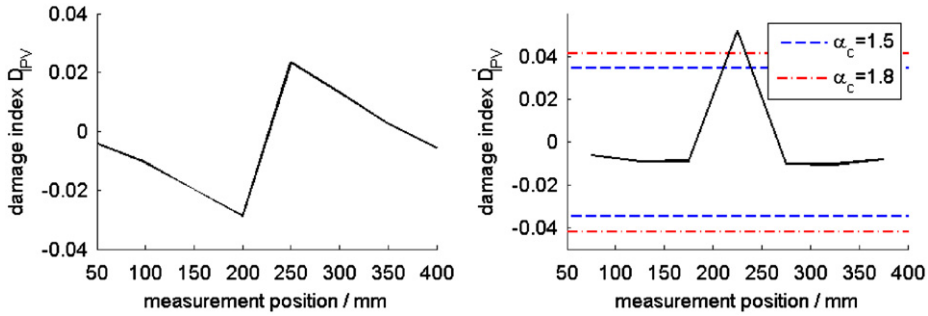

Fig. 15. Damage detection results of structure state D21 (debonding location is between 200 and 250 mm).

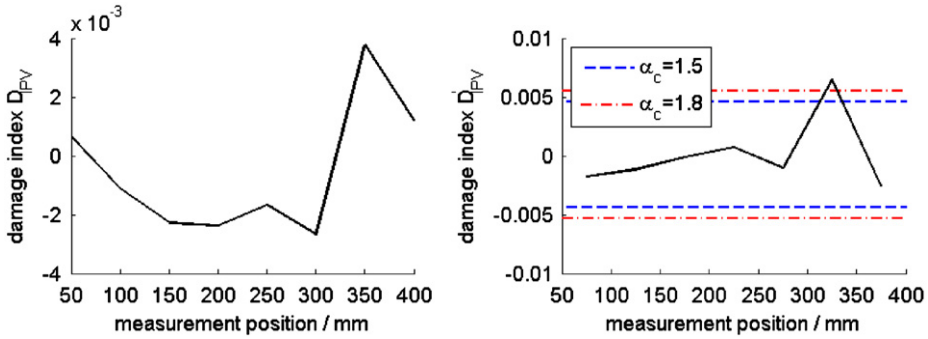

Fig. 16. Damage detection results of structure state D31 (debonding location is between 300 and 350 mm).

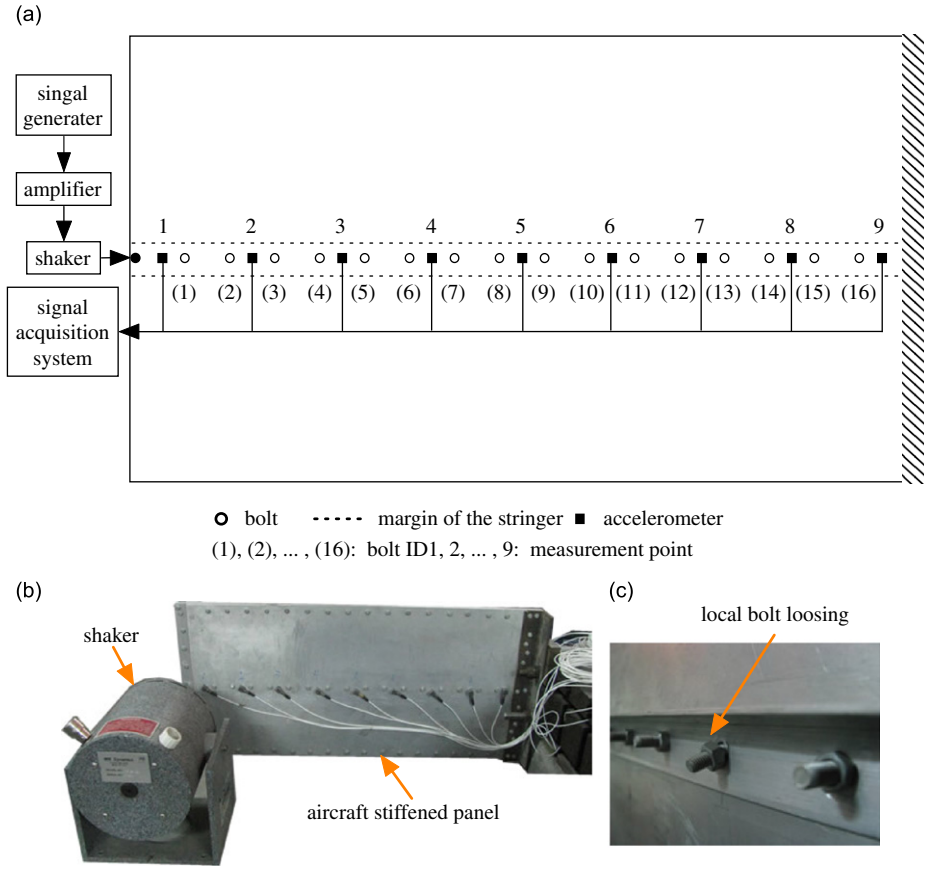

Fig. 17. Aircraft stiffened panel and test setup: (a) sketch of test setup, (b) test setup and (c) loosening of bolt.

occurring on the interface between the stringers and the panel is simulated by the loosening of bolt. In the experiment, the aircraft stiffened panel is excited by an electromagnetic shaker at the middle of the free end of the panel, and 9 accelerometers are affixed along the stringers with identical interval, i.e. there are two bolts between each two accelerometers, as shown in Fig. 17. Four different structure states with different bolt loosenings are simulated, as listed in Table 3.

The first two natural frequencies of the intact aircraft stiffened panel can be easily measured by the sweep sine method, and they are 10.27 and 53.15 Hz. The accelerations of the intact structure and each simulated structure states are measured under 0–20 Hz (which covers the fundamental natural frequency of the structure) band pass white noise excitations, and then the IPVs and the corresponding damage index are calculated; finally the damage in each simulated structure state is located. In the experiment, the reference response measurement point for calculating IPVs is the measurement point at the free end of the panel (i.e. measurement point 1). Meanwhile, it is found that the abrupt change

Table 3
Simulated structure states of the aircraft stiffened panel.

Structure state	D1	D2	D3	D4
Loosening bolt ID	(2)	(6)	(10)	(14)
Corresponding measurement point	2	4	6	8

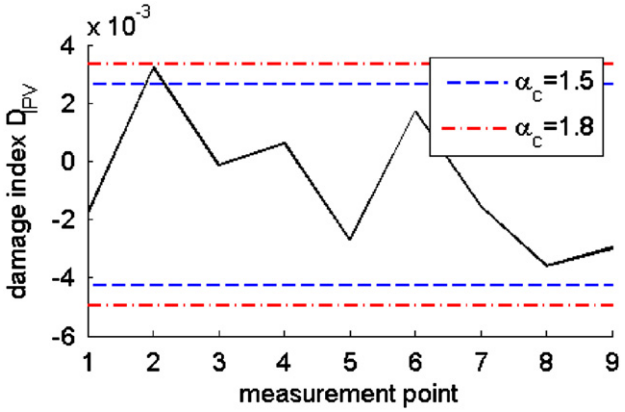

Fig. 18. Damage detection results of structure state D1 (loosening bolt ID is (2) and the corresponding measurement point is 2).

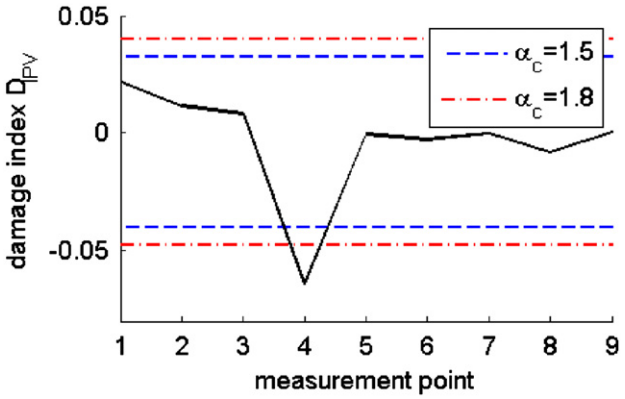

Fig. 19. Damage detection results of structure state D2 (loosening bolt ID is (6) and the corresponding measurement point is 4).

in $\mathbf{D}_{IPV}$ of honeycomb sandwich composite beam is "impulse change"; thus the local maximum of $\mathbf{D}_{IPV}$ is utilized to locate the damage, and the confidence interval factor α_c is set as 1.5 or 1.8.

Figs. 18–21 show the damage detection results of structure states D1, D2, D3 and D4 of the aircraft stiffened panel. As shown in these figures, structure states D2, D3 and D4 of the aircraft stiffened panel are correctly detected by the IPV-based structural damage detection method using the confidence interval factor α_c as 1.5 or 1.8. For structure state D1, the damage is correctly detected when the confidence interval factor α_c is 1.5, but false negative detection occurs when the confidence interval factor α_c is 1.8. The reason for the false negative detection occurring in structure state D1 is that the effect of local damage simulated in structure state D1 on the lower modes is slight as the loosening bolt is far from the clamped end of the panel, i.e. structure state D1 is very close to the intact structure. In conclusion, using the acceleration responses under 0–20 Hz band pass white noise excitation and setting the confidence interval factor α_c as 1.5 or 1.8, the IPV-based structural damage detection method can be utilized to correctly locate the bolt loosening location in the aircraft stiffened panel.

5. Conclusions

The theory of inner product vector and its application to structural damage detection have been investigated. The IPV was defined by the cross correlation functions of the responses under white noise excitation. As the ideal white noise with

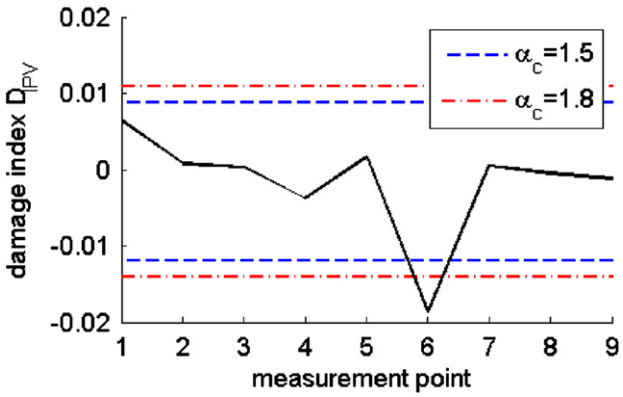

Fig. 20. damage detection results of structure state D3 (loosening bolt ID is (10) and the corresponding measurement point is 6).

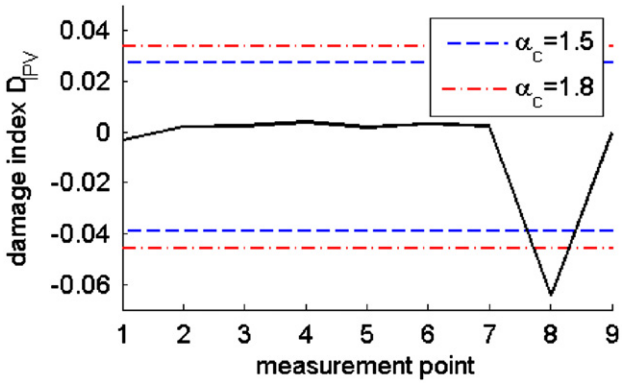

Fig. 21. damage detection results of structure state D4 (loosening bolt ID is (14) and the corresponding measurement point is 8).

unlimited bandwidth is nonexistent, the IPV calculated by the time domain vibration response under band pass white noise is further investigated in this paper. It is theoretically proved that the IPV, which can be calculated by displacement, velocity and acceleration, is a weighted summation of mode shapes of the structure. It is also proved that the effect of some particular measurement noise can be adaptively eliminated in the calculation of IPV.

Based on the fact that the IPV is a weighted summation of mode shapes of the structure, the IPV-based structural damage detection method is proposed, and the damage is located by the abrupt changes in the damage index defined by the changes in IPV of the intact and damaged structure. The threshold for damage detection is utilized to distinguish the changes in IPV caused by damage and various errors. The feasibility and effectiveness of the IPV-based structural damage detection method are illustrated by three damage detection experiments, i.e. stiffness reduction detection of shear frame structure, debonding damage detection of honeycomb sandwich composite beam and bolt loosening detection of the aircraft stiffened panel.

As the damage detection procedure is rather simple, and is just utilizing the time domain vibration responses under band pass white noise excitation, the IPV-based damage detection method can be used as an online damage detection method. However, like many of the existing damage detection methods, the relations between abrupt changes in the damage index and damage extent are rather complex; the IPV-based structural damage detection method cannot be utilized to evaluate the damage extent quantitatively. Meanwhile, the other shortage of the IPV-based structural damage detection method is the cost of sensors, which means that the sensor should be located close to the damage.

Acknowledgements

This work was funded by the Project of New Century Excellent Talents Granted by the Ministry of Education of the People's Republic of China (Grant No. NCET-04-0965) and 111 Project of the People's Republic of China (No. B07050). The authors are also grateful to Prof. Paul White for his help in deducing some formulae, and to Miss Yan Ding and Mr. Muyu Zhang for their help in conducting the experiments.

References

[1] S.W. Doebling, C.R. Farrar, M.B. Prime, et al., Damage identification and health monitoring of structural and mechanical systems from changes in their vibration characteristics: a literature review. Los Alamos National Laboratory Report LA-13070-MS, 1996.
[2] H.S. Sohn, C.R. Farrar, F.M. Hemez, et al., A review of structural health monitoring literature: 1996–2001. Los Alamos National Laboratory Report LA-13976-MS, 2003.
[3] C.R. Farrar, K. Worden, M.D. Todd, et al., Nonlinear system identification for damage detection. Los Alamos National Laboratory Report LA-14351-MS, 2007.
[4] C.R. Farrar, K. Worden, An introduction to structural health monitoring, *Philosophical Transactions of the Royal Society A* 365 (2007) 303–305.
[5] X.Y. Li, S.S. Law, Damage identification of structures including system uncertainties and measurement noise, *AIAA Journal* 46 (1) (2008) 263–276.
[6] J. Park, Identification of damage in beam structures using flexural wave propagation characteristics, *Journal of Sound and Vibration* 318 (2008) 820–829.
[7] M. Dilena, A. Morassi, Vibrations of steel–concrete composite beams with partially degraded connection and applications to damage detection, *Journal of Sound and Vibration* 320 (2009) 101–124.
[8] S.J. Dyke, B.H. Koh, Structural health monitoring for flexible bridge structures using correlation and sensitivity of modal data, *Computers and Structures* 85 (2007) 117–130.
[9] L. Yu, L. Cheng, L.H. Yam, et al., Online damage detection for laminated composite shells partially filled with fluid, *Composite Structures* 80 (2007) 334–342.
[10] M.I. Friswell, J.E. Mottershead, in: *Finite Element Model Updating in Structural Dynamics*, Kluwer Academic Publishers, London, 1999, pp. 63–71.
[11] A.N. Tikhonov, V.Y. Arsenin, in: *Solution of Ill-Posed Problems*, Winston & Son, Washington, DC, 1977.
[12] J. –T. Kim, Y. –S. Ryu, H. –M. Cha, et al., Damage identification in beam-type structures: frequency-based method vs mode-shape-based method, *Engineering Structures* 25 (2003) 57–67.
[13] M. Dilena, A. Morassi., The use of antiresonances for crack detection in beams, *Journal of Sound and Vibration* 276 (2004) 195–214.
[14] A. Alvandi, C. Cremona, Assessment of vibration-based damage identification techniques, *Journal of Sound and Vibration* 292 (2006) 179–202.
[15] S. Choi, S. Park, N.-H. Park, et al., Improved fault quantification for plate structure, *Journal of Sound and Vibration* 297 (2006) 865–879.
[16] W.O. Wong, X.Q. Wang, L. Cheng, Modal power flow analysis of a damaged plate, *Journal of Sound and Vibration* 320 (2009) 84–100.
[17] K. Worden, G. Manson, N.R. Fieller, Damage detection using outlier analysis, *Journal of Sound and Vibration* 229 (3) (2000) 647–667.
[18] G. Manson, K. Worden, D.J. Allman, Experimental validation of a structural health monitoring methodology. Part III: damage location on a gnat aircraft, *Journal of Sound and Vibration* 259 (2) (2003) 365–385.
[19] S.G. Pierce, K. Worden, G. Manson., A novel information-gap technique to assess reliability of neural network-based damage detection, *Journal of Sound and Vibration* 293 (2006) 96–111.
[20] S.S. Wang, Q.W. Ren, Structure damage detection using local damage factor, *Journal of Vibration and Control* 12 (9) (2006) 955–973.
[21] S.D. Fassois, J.S. Sakellarou, Time-series methods for fault detection and identification in vibrating structures, *Philosophical Transactions of the Royal Society A* 365 (2007) 411–448.
[22] I. Trendafilova, E. Manoach, Vibration-based damage detection in plates by using time series analysis, *Mechanical Systems and Signal Processing* 22 (2008) 1092–1106.
[23] Z.C. Yang, L. Wang, H. Wang, et al., Damage detection in composite structures using vibration response under stochastic excitation, *Journal of Sound and Vibration* 325 (4–5) (2009) 755–768.
[24] G.H. James III, T.G. Carne, J.P. Lauffer, The Natural Excitation Technique (NExT) for modal parameter extraction from operating structures, *Modal Analysis: The International Journal of Analytical and Experimental Modal Analysis* 10 (4) (1995) 260–277.
[25] G.H. James. III, C.R. Farrar, System identification from ambient vibration measurements on a bridge, *Journal of Sound and Vibration* 205 (1) (1997) 1–18.
[26] J.S. Bendat, A.G. Piersol, in: *Random Data: Analysis and Measurement Procedures*, 3rd ed, , 2000.
[27] A. Papoulis, S.U. Pillai, in: *Probability, Random Variables and Stochastic Processes*, 4th ed, McGraw-Hill, New York, 2002.
[28] J.-T. Kim, N. Stubbs, Crack detection in beam-type structures using frequency data, *Journal of Sound and Vibration* 259 (1) (2003) 145–160.
[29] A.-M. Yan, G. Kerschen, P.D. Boe, et al., Structural damage diagnosis under varying environmental conditions—part I: a linear analysis, *Mechanical Systems and Signal Processing* 19 (2005) 847–864.